Explanation of core ion cyclotron emission from beam-ion heated plasmas in ASDEX Upgrade by the magnetoacoustic cyclotron instability

Lunan Liu[1, 2], R. Ochoukov[3], K.G. McClements[4], R.O. Dendy[4, 5], V. Bobkov[3], M. Weiland[3], R. Bilato[3], H. Faugel[3], D. Moseev[6], M. Salewski[7], Wei Zhang[3], Xinjun Zhang[2], Yubao Zhu[8], B. Chapman[4], A. Zalzali[5], ASDEX Upgrade Team[a] and EUROfusion MST1 Team[b]

[1] College of Physics and Optoelectronic Engineering, Shenzhen University, Shenzhen 518060, China
[2] Institute of Plasma Physics, Chinese Academy of Sciences, Hefei, 230031, China
[3] Max Planck Institute for Plasma Physics, Boltzmannstr. 2, D-85748 Garching, Germany
[4] Culham Centre for Fusion Energy, Culham Science Centre, Abingdon, Oxfordshire, OX14 3DB, UK
[5] Centre for Fusion, Space and Astrophysics, University of Warwick, Coventry, CV4 7AL, United Kingdom
[6] Max Planck Institute for Plasma Physics, Wendelsteinstra. 1, D-17491 Greifswald, Germany
[7] Technical University of Denmark, Department of Physics, DK-2800 Kgs. Lyngby, Denmark
[8] Hebei Key Laboratory of Compact Fusion, Langfang 065001, China
[a] See the author list in [39]; [b] See the author list in [40]

E-mail: liulunan@ipp.ac.cn

Abstract

Bursts of ion cyclotron emission (ICE), with spectral peaks corresponding to the hydrogen cyclotron harmonic frequencies in the plasma core are detected from helium plasmas heated by sub-Alfvénic beam-injected hydrogen ions in the ASDEX Upgrade tokamak. Based on the fast ion distribution function obtained from TRANSP / NUBEAM code, together with a linear analytical theory of the magnetoacoustic cyclotron instability (MCI), the growth rates of MCI could be calculated. In our theoretical and experimental studies, we found that the excitation mechanism of core ICE driven by sub-Alfvénic beam ions in ASDEX Upgrade is MCI as the time evolution of MCI growth rates is broadly consistent with measured ICE amplitudes. The MCI growth rate is very sensitive to the energy and velocity distribution of beam-injected ions and is suppressed by the slowing down of the dominant beam-injected ion velocity and the spreading of the fast ion distribution profile. This may help to account for the experimental observation that ICE signals disappear within ~3 ms after the NBI turn-off time, much faster than the slowing down times of the beam ions.

Keywords: Magnetoacoustic Cyclotron Instability, Ion Cyclotron Emission, Sub-Alfvénic Beam Injected Ions, ASDEX Upgrade Tokamak

1. Introduction

Ion cyclotron emission (ICE) driven by energetic ions is one kind of electromagnetic radiation whose spectrum peaks correspond to the harmonics of the cyclotron frequencies of energetic ion species near the emission location. Typically, but not perpetually, ICE is observed to be excited at the outer edge of the plasma in toroidal magnetically confined fusion devices, such as JET [1, 2], TFTR [3, 4], JT-60U [5], ASDEX Upgrade [6], DIII-D [7], KSTAR [8, 9], EAST [10] and LHD

[11]; ICE from the plasma core has been described at a recent time from DIII-D[12], ASDEX Upgrade [6, 13-15] EAST [16] and small tokamak TUMAN-3M [17], and earlier from JT-60U [18].

The ICE is thought to be excited by energetic ions which have a positive gradient in the velocity direction (bump-on tail structure) and have a very intense pitch angle anisotropy [19]. Neutral beam populations at ASDEX Upgrade have this structure according to TRANSP / NUBEAM and measurements by velocity-space tomography [20-23]. The magnetoacoustic cyclotron instability (MCI) excited from the resonance interaction of energetic ions and fast magnetoacoustics waves is recommended as a probable emission mechanism for the ICE [24-34]. The fast ion cyclotron resonance condition with a Doppler-shift in the vicinity of the l^{th} cyclotron harmonic is given by, $\omega - l\Omega_f = k_{//}v_{f//}$, where ω is the wave angular frequency, l is the positive integer, Ω_f is the ion Larmor cyclotron angular frequency, $k_{//}$ is the parallel wavenumber, $v_{f//}$ is the fast ion's parallel velocity [35].

Previously, in ASDEX Upgrade, it was found that the amplitude of second harmonic of ICE from the core plasma heated by sub-Alfvénic beam-injected ions is consistent with the growth rate of MCI which is a result of competition between the beam ion fraction build-up and dominant beam ion velocity component slowing down [30]. Based on previous work, we present some new experimental evidence in ASDEX Upgrade to further demonstrate that the core ICE driven by sub-Alfvénic beam injected ions is attributed to the MCI. The rest of the paper is organized as follows: the experimental setup is presented in section 2, then the experimental results are described in section 3, followed by section 4 which focuses on theoretical modeling and simulation results, and we conclude with a summary in the last section.

2. Experimental setup

ASDEX Upgrade is a tokamak with a major radius of $R = 1.6$ m, and a minor radius $r = 0.5$ m [36]. In shot 36719, the plasma current I_p flows anti-clockwise as shown in figure 1, and the direction of the magnetic field B_t is clockwise. The outermost and innermost closed magnetic surfaces are shown as blue circles labeled as separatrix. The green circle stands for the magnetic axis. Two neutral beam injection (NBI) sources were used in our experiments, the bold black / red straight line represents NBI-8 / NBI-3. A low field-side B-dot probe used to detect ICE signals is shown as a purple circle dot. The ICE signal from the B-dot probe has been divided into two signals, one signal is connected to a filter with bandpass 10–50 MHz and used to obtain the time evolution of rectified ICE intensity by low-speed acquisition card (200 kHz); the other signal is connected to high-speed acquisition system (200 MHz / s) to extract the frequency spectrum of ICE. Here, we want to point out that the fast speed acquisition system works once in 1 millisecond (ms) and collect 16384 points a time using about 0.082 ms. The spectrum of ICE could be calculated by performing Fast Fourier Transform using those 16384 points (~0.084 ms).

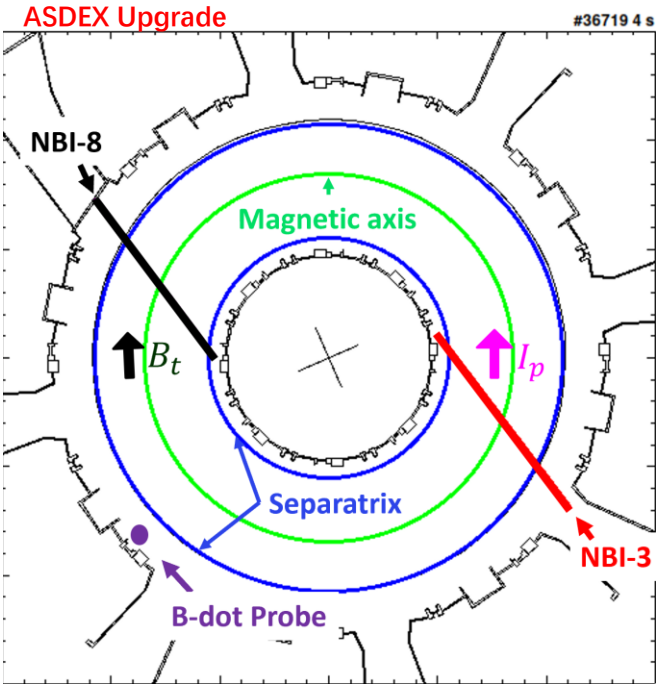

Figure 1. The top view of ASDEX Upgrade. In shot 36719, plasma current I_p flows anti-clockwise, the direction of toroidal magnetic field B_t is clockwise. The position of magnetic axis, closed magnetic surface separatrix, B-dot probe, and the geometry of two neutral beams injection (NBI) are shown.

3. Experimental results

In shot 36719, L-mode, core ICE is detected in helium plasma only heated with hydrogen NBI. The NBI power is shown in figure 2(a), 1.8 MW NBI-3 shown as the red line with 52 keV particle energy, and 1.5 MW NBI-8 shown as the black line with 71 keV particle energy. Each NBI pulse is 10 ms in duration and spaced apart by 26 ms, NBI-3 and NBI-8 work alternately. From the magnetic field (figure 2(g)) and the core plasma density (figure 2(f)), the Alfvénic speed $c_A \sim 6.28 \times 10^6$ m / s could be calculated, so the beam-injected hydrogen ions in our experiments are sub-Alfvénic ions as the velocity of 52 keV (71 keV) beam ion is 3.16×10^6 m / s (3.69×10^6 m / s). The on-axis magnetic field $B_{on-axis}$ is around 2.4 T with two small downward steps at the time of $t = 2.6$ s and $t = 3.6$ s shown in figure 2(g). The core plasma density is $n_e \approx 3.5 \times 10^{19}$ m^{-3} shown in figure 2(f).

Spectrum splitting occurs at both the fundamental and second harmonic frequencies of ICE shown in figure 2(c) and figure 2(d), the fundamental frequency of ICE is mainly located around $f_1 \sim 38.2$ MHz and the second harmonic frequency of ICE is mainly located around $f_2 \sim 75.2$ MHz, $f_3 \sim 76.4$ MHz shown in figure 2(d) is exactly double the frequency value of $f_1 \sim 38.2$ MHz. Matching the ICE and hydrogen ion cyclotron resonance frequency and from the fact that only fast beam-injected hydrogen ions can appear in helium plasmas heated by hydrogen NBI, so the ICE is excited by beam-injected hydrogen ions in the plasma core. It is obviously that the ICE frequency (figure 2(c), (d)) follows the magnitude of the on-axis magnetic field $B_{on-axis}$ (figure 2(g)). The equation of ion Larmor cyclotron frequency is $f = \frac{B}{2\pi} \times \frac{|q|}{m}$ (B is the magnetic field, $\frac{|q|}{m}$ is the charge-mass ratio of ion). For hydrogen ions, using the value of on-axis total magnetic field $B_{on-axis}$, we can get the hydrogen ion Larmor cyclotron frequency on the magnetic axis ($f \sim 37$ MHz) which is ~ 1 MHz lower comparing with the fundamental frequency ($f_1 \sim 38.2$ MHz) of ICE shown in figure 2(c). Here, two assumptions are proposed as explanations for the 1 MHz difference between ICE and ion Larmor cyclotron frequencies. First, the ICE frequency is influenced by Doppler-shift ($k_{//} v_{f//} \neq 0$); second, the beam-injected fast ions are not accurately focused on the magnetic axis as 5 cm radial movement of fast ions can cause 1 MHz frequency difference. The time evolution of ICE amplitude in the frequency range of 10 MHz - 50 MHz is shown in figure 2(b), and this signal only includes the fundamental frequency of ICE.

According to the previous description, in shot 36719, there are two neutral beams with different particle energies. To study the relationship between ICE amplitude and the energy of fast ions, the ICE amplitude had be analysed in one cycle shown in figure 3 which is zoomed in the left side of figure 2 during the time of 2.19 s - 2.25 s. Fine structures of ICE amplitude and NBI power are shown in figure 3 (b) and (a) respectively, it is clear that the ICE amplitude is much larger with 71 keV NBI-8 (1.5 MW) even though the power of it is lower compared to 52 keV NBI-3 (1.8 MW). So, we can conclude that ICE signal intensity is more sensitive to the NBI energy (and, hence, ions speed value) than to the NBI power. To illustrate this conclusion further, the histogram graph [37] of ICE energy (E) calculated based on ICE power (P(t)) (figure 2(b)) in each NBI pulses is shown in figure 4 ($E = \int_{t_0}^{t_0+0.01s} P(t) \times tdt \approx \sum_{i=1}^{i=163840} P_i \times \frac{1}{16384000}$, 16384000 is the sampling rate of fast speed acquisition system, t_0 is the start time of the NBI pulse, 0.01 s is the duration time of NBI pulse, $P_1 = P(t_0)$). The X-axis corresponds to ICE energy in each NBI pulses, and the Y-axis represents the probability of a specific ICE energy value. It is obviously that the dominant part of ICE energy with 71 keV NBI-8 (1.5 MW) is three times larger than that with 52 keV NBI-3 (1.8 MW).

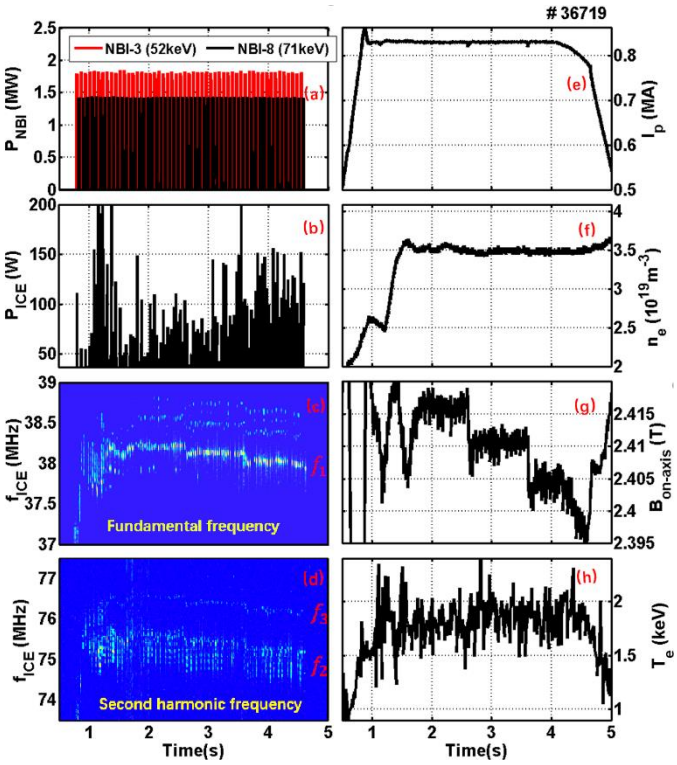

Figure 2. Time evolution of key discharge parameters and ion cyclotron emission (ICE) signal in shot 36719, helium plasma heated by hydrogen NBI. (a) Neutral beams injection (NBI) power, 52 keV NBI-3 (1.8 MW) is shown as red curve, 71 keV NBI-8 (1.5 MW) is shown as black curve; (b) ICE amplitude; (c) (d) corresponding to fundamental and second harmonic frequencies of ICE spectrum; (e) plasma current I_p; (f) electron density n_e; (g) on-axis toroidal magnetic field $B_{on-axis}$; (h) the core electron temperature T_e.

From figure 3, it is clear that both the fundamental (figure 3(b), (c)) and the second harmonic frequencies (figure 3(d)) of ICE disappear rapidly after the NBI turn-off. In order to display this phenomenon in detail, the ICE signals in figure 3(c), (d) during 2.206 s -2.212 s (in the black rectangle) and 2.242 s – 2.248 s (in the red rectangle) are expanded as shown in figure 5. It is the time evolution of the ICE amplitudes (from the high-speed acquisition system) around the end of NBI. From these four curves in figure 5 (a) and (b), it is clear that both the fundamental and the second harmonic frequencies of core ICE signals fall off extremely fast after the NBI turn-offs (less than 3 ms): NBI-8 (71 keV) turn-off at t = 2.208 s and NBI-3 (52 keV) turn-off at t = 2.244 s. As a comparison, the slowing-down time of beam-injected high-energy hydrogen ions in plasma core is more than 30 ms. Previously [30], it is described that the second harmonic of the core ICE excited by sub-Alfvénic deuterium beam-injected ions disappears within 1 ms after the NBI turn-off. In EAST tokamak, a similar observation for the fundamental frequency of core ICE had been reported [16]. From figure 5, it is also clear that the ICE signal at the fundamental frequency is approximately 10 times larger than that at the second harmonic.

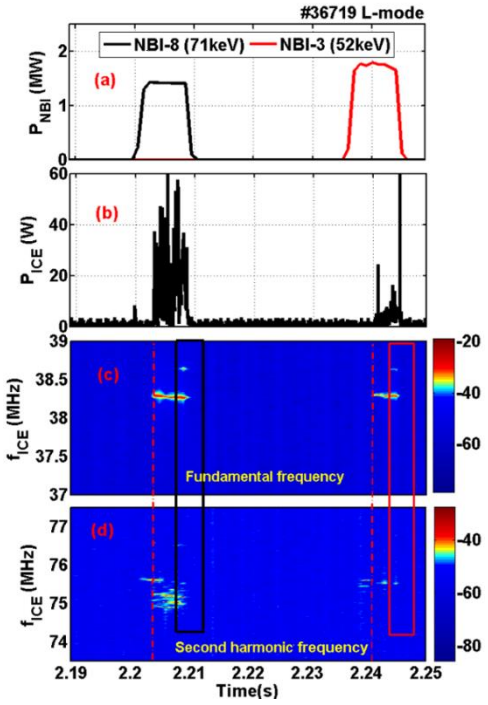

Figure 3. An example of (a) NBI power, (b) ICE amplitude, (c) fundamental and (d) second harmonic frequencies of ICE spectrum in one cycle zoomed in the left side of figure 2 during 2.19 s – 2.25 s. In figure (d), the pre-appearing second harmonic of ICE appears ~ 2 ms earlier than the fundamental frequency (in front of the red dashed line).

From the core ICE spectrum shown in figures 3(c) and 3(d), we observe, first, that the ICE does not appear instantaneously after NBI turn-on. This reflects the fact that time is needed for the beam-ion fraction to build up, and such behaviour is also observed in paper [30]. Second, we observe that the ICE signal at the second harmonic frequency appears ~ 2 ms earlier than that at the fundamental frequency, and the earlier part is in front of the red dashed line shown in figure 3(c) (d), hereafter we refer to this component of the ICE spectrum as pre-appearing ICE. As described in the paper [30], the beam ion fraction build-up is a prerequisite for the appearance of this kind of ICE. So, one possible reason for the appearance of pre-appearing ICE could be that the second harmonic ICE has a lower requirement in beam ion fraction build-up. Further theoretical studies are needed to comprehensively describe this phenomenon.

So far, we have talked about several phenomena of core ICEs driven by sub-Alfvénic beam injected ions in ASDEX Upgrade: (1) the ICE amplitude is larger with 71 keV NBI-8 (1.5 MW) even though the power of it is lower compared to 52 keV NBI-3 (1.8 MW); (2) the ICEs (fundamental or second harmonic frequency) disappear immediately after NBI turn-off; (3) the ICE signal at the fundamental frequency is about ten times larger than that at the second harmonic frequency; (4) the pre-appearing ICE signal appears ~ 2 ms earlier than ICE signal at the fundamental frequency. In the next section, the MCI growth rate is calculated based on the fast beam-injected ions distributions in the plasma core simulated by TRANSP / NUBEAM [30].

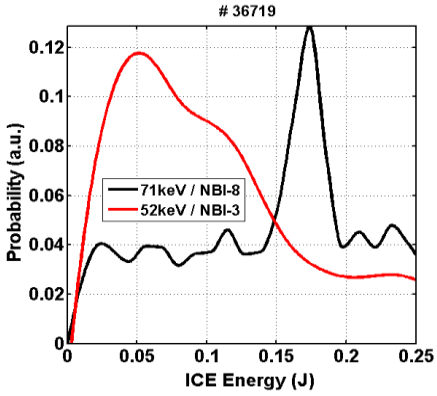

Figure 4. The histogram graph of ICE energies distribution, the X-axis stands for ICE energies in one NBI pulse, the Y-axis stands for the possibility in a specific ICE energy value, the red line corresponding to 52 keV NBI-3, the black line corresponding to 71 keV NBI-8.

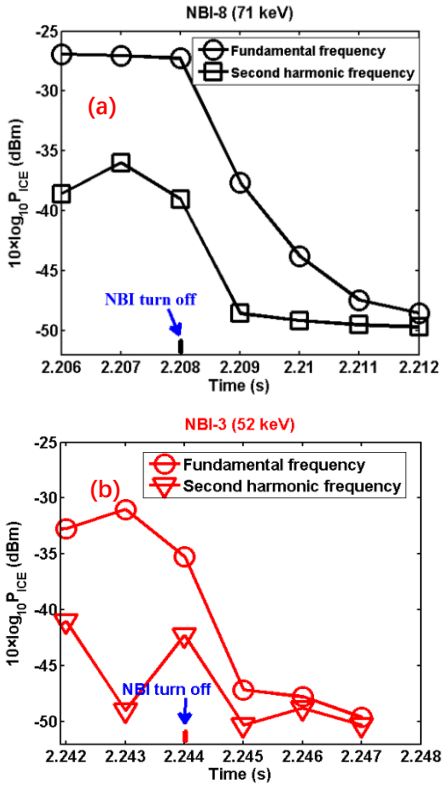

Figure 5. The time evolution of the ICE amplitudes around the end of NBI, ICE amplitude is from the high-speed acquisition system. (a) A detail view of ICE amplitudes during 2.206 s - 2.212 s corresponding to the black rectangle in figure 3, NBI-8 turning off at t = 2.208 s; (b) a detail view of ICE amplitudes during 2.242 s - 2.248 s corresponding to the red rectangle in figure 3, NBI-3 switching off at t = 2.244 s.

4. **Theoretical modelling and simulation results discussion**

The excitation mechanism for ICE is proposed as MCI which can be driven when energetic ions interact with the fast Alfvénic wave propagating obliquely with respect to the local magnetic field. The linear analytical theory of the MCI is derived from the dispersion relation of the fast Alfvénic wave that was obtained by using Maxwell equations and dielectric tensor elements [25, 26]. Based on previous paper [30], together with a richer set of experimental results of ICE described in the last chapter, more pieces of evidence are provided to prove that the excitation mechanism for core ICE driven by beam-injected ions in ASDEX Upgrade is MCI.

According to previous studies [25, 26, 31, 32], a suitable ring-like distribution model for energetic ions in the emitting region is successfully used to obtain the appropriate dispersion relation of obliquely propagating fast Alfvénic waves. The equation for that kind of energetic ions distribution model is written as [38]:

$$f = \frac{1}{2\pi^{3/2} u v_r} \exp\left(-\frac{(v_{//}-v_d)^2}{v_r^2}\right)\delta(v_\perp - u) \quad (1)$$

This is a normalized equation, where $v_{//}$ is the parallel velocity component which has a drifting Maxwellian distribution, and $v_\perp$ is perpendicular velocity component which has a delta distribution function, and v_r, v_d and u are constants defined as parallel velocity spread, average parallel drift speed and perpendicular speed of the energetic ions. In this paper, we assume that the beam injected fast hydrogen ions distribution in ASDSEX Upgrade tokamak can be approximated as ring-like distribution. Then, those three constants could be calculated based on TRANSP / NUBEAM module [30].

Using the distribution function of energetic ions corresponding to equation (1), the growth or damping rate of obliquely-propagating MCI γ can be obtained [25, 26]. The expression equation of γ is shown below as:

$$\gamma = \frac{\omega_{pb}^2}{\omega_{pi}^2} \frac{\Omega_i^4}{\left[\Omega_i+(\omega-\Omega_i)N_{//}^2\right]\left[\Omega_i-(\omega+\Omega_i)N_{//}^2\right]} \times \left(\frac{l\Omega_b}{k_{//}v_r} M_l - \frac{2u^2}{v_r^2}\eta_l N_l\right)\frac{\sqrt{\pi}}{2\omega} e^{-\eta_l^2} \quad (2)$$

In the growth / damping rate of equation (2), γ deriving, the wave electric field is approximately polarized in the plane perpendicular to the direction of the magnetic field, which means that we neglect the influence of Landau damping (from electron or ion). Furthermore, the ratio of energetic ions (n_b) to plasma density (n_i) $\xi = n_b/n_i$ is supposed to be small. In equation (2), Ω corresponding to cyclotron frequency and ω_p standing for plasma frequency, the subscripts i and b refer to bulk and beam-injected energetic ions; $N_{//} = k_{//}c_A/\omega$, where ω and $k_{//}$ are the mode frequency and parallel wave number; $\eta_l = (\omega - k_{//}v_d - l\Omega_b)/k_{//}v_r$, l is an integer; the expression of M_l and N_l are defined as follows:

$$M_l = 2l\frac{\omega}{\Omega_l}\left(J_l'^2 + \frac{1}{z_b^2}(l^2 - z_b^2)J_l^2\right) - 2\frac{\omega^2-\Omega_i^2}{\Omega_i^2}\frac{J_l J_l'}{z_b}\left[l^2 N_\perp^2 - (z_b^2 - 2l^2)N_{//}^2\right] + \frac{2J_l J_l'}{z_b}(z_b^2 - 2l^2) \quad (3)$$

$$N_l = -2l\frac{\omega}{\Omega_i}\frac{J_l J_l'}{z_b} + \frac{\omega^2-\Omega_i^2}{\Omega_i^2}\left[N_{//}^2\left(\frac{l^2 J_l^2}{z_b{}^2} + J_l'^2\right) + N_\perp^2\frac{l^2 J_l^2}{z_b{}^2}\right] + \frac{l^2 J_l^2}{z_b^2} + J_l'^2 \quad (4)$$

In this expression $N_\perp = k_\perp c_A/\omega$, $k_\perp$ is the perpendicular wave number, J_l denotes the Bessel function of order l and with an argument $z_b = k_\perp u/\Omega_b$, and J_l' corresponding to the first derivative of J_l. The positive value of γ represents destabilizing. As discussed in [25, 26], N_l is generally positive, to make sure $\gamma > 0$, η_l should be negative which means $\omega - k_{//}v_d < l\Omega_b$. M_l is usually negative in the sub-Alfvénic regime $u < c_A$ (for beam-injected ions in ASDEX Upgrade, this is satisfied). The above description of the MCI growth rate is only valid with $k_{//} > 0$. The expression must be modified for negative parallel wavenumbers.

If the propagation direction of the fast Alfvénic wave and fast ions distribution functions are already calculated, the growth / damping rate γ could be expressed as a function of fast Alfvénic wave frequency $\gamma = \gamma(\omega)$. Here, a nearly perpendicular propagation angle of $\theta = 84°$ is chosen, and we will prove that this is an appropriate choice lately. The dispersion relation of the fast Alfvénic wave is described as [25]:

$$\omega^2 = \frac{1}{2}c_A^2\left[k^2 + k_{//}^2 + k^2 k_{//}^2\frac{c_A^2}{\Omega_i^2} + \sqrt{\left(k^2 + k_{//}^2 + k^2 k_{//}^2\frac{c_A^2}{\Omega_i^2}\right)^2 - 4k^2 k_{//}^2}\right] \quad (5)$$

Then, the parallel wavenumber could be described as $k_{//} = k * \cos(84°)$, the perpendicular wave number could be described as $k_\perp = k * \sin(84°)$.

Now we start to calculate the constants v_d, v_r and u in

the energetic ion distribution equation (Eq. (1)) based on the energetic ions distribution simulated from TRANSP / NUBEAM. The energetic ions distribution functions in pitch-energy space of shot 36719 at 2.206 s (with 71 keV NBI-8) and 2.242 s (with 52 keV NBI-3) are shown in figure 6, it is clear that the dominant pitch value (v_d/v_{total}) is 0.5 at 2.206 s and 0.54 at 2.242s. Then, the values of two constants $v_d = \sqrt{\frac{2E_{dominant}}{m_b}} \times$ pitch angle and $u = \sqrt{\frac{2E_{dominant}}{m_b} - v_d^2}$ could be calculated based on the dominant part of energetic ions corresponding to $E_{dominant}$ shown as red dashed line in figure 6. From TRANSP / NUBEAM simulation results, the ratio of energetic ions (n_b) to plasma density (n_i) $\xi = n_b/n_i$ around the $E_{dominant}$ also could be calculated. At t = 2.206 s, the ratio ξ is about 1.7×10^{-3}; at t = 2.242 s, the ratio ξ is about 3.6×10^{-3}, it satisfied the assumption that ξ should be small.

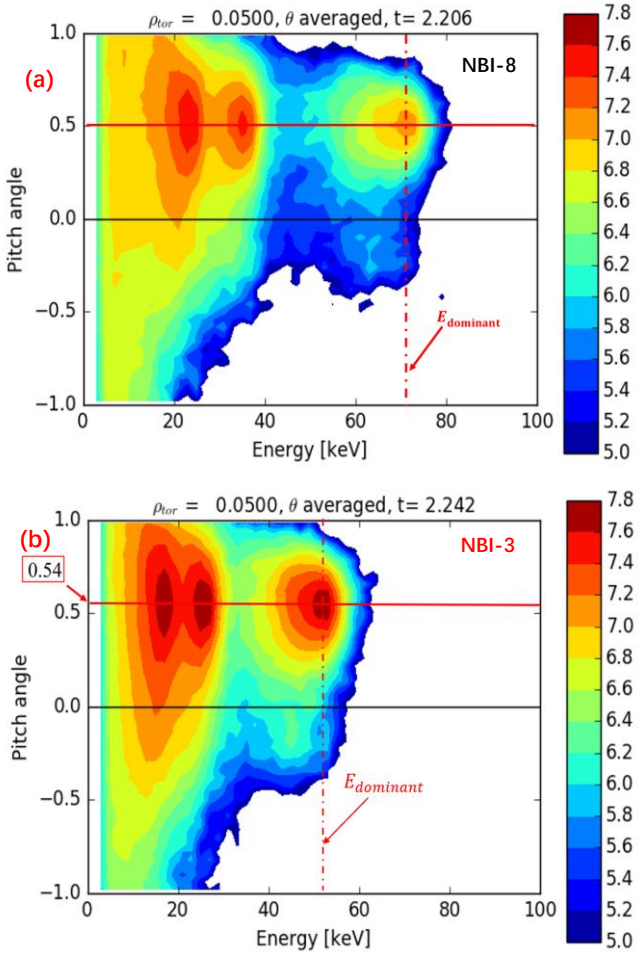

Figure 6. Beam-ions pitch-energy distribution function in the plasma core ($\rho_{tor} = 0.05$). The full, half and 1/3 $E_{dominant}$ (red dashed line) components of the beam-injected ions correspond to the three peaks clearly shown in the picture. (a) Corresponding to t = 2.206 s (the start time of figure 5 (a)) with 71 keV NBI-8 (1.5 MW), the pitch angle is dominant in 0.5 corresponding to the red line; (b) corresponding to t = 2.242 s (the start time of figure 5 (b)) with 52 keV NBI-3 (1.8 MW), the pitch angle is dominant in 0.54.

The beam-injected ions distribution function in energy space with a specific pitch angle is shown in figure 7 (a) and (b) corresponding to t = 2.206 s with 71keV NBI-8 (1.5 MW) and to t = 2.242 s with 52 keV NBI-3 (1.8 MW) respectively. Figure 7(a) / (b) is from figure 6(a) / (b) with pitch value = 0.5 / 0.54. The fast ion energies corresponding to half the maximum of distribution function 1/2 f_{max}, are defined as E_{max} and E_{min} shown in figure 7. Then we can get the parallel velocity spread of the energetic ions $v_r = \sqrt{\frac{2E_{max}}{m_b}} - \sqrt{\frac{2E_{min}}{m_b}}$, m_b is the mass of beam ions which is hydrogen ions in this manuscript. Here, only the full $E_{dominant}$ component of the beam-injected ions is concerned as the influence of the half, and the 1/3 $E_{dominant}$ components on MCI could be neglected compared to full $E_{dominant}$. So far, based on the fast ion distribution function from TRANSP / NUBEAM shown in figure 6 and 7, all the parameters in the distribution function of energetic ions, and the ratio between the fast ion density and the plasma density ξ are successfully calculated.

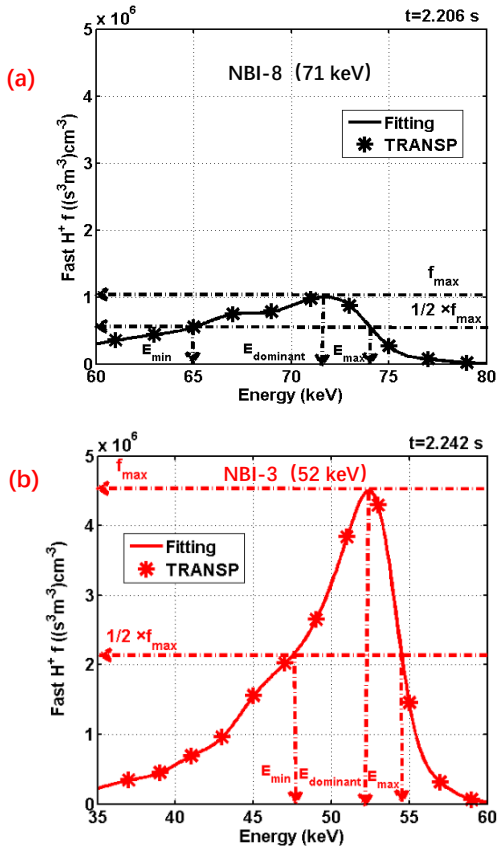

Figure 7. TRANSP-calculated beam ion energy distribution with a specific pitch value, the f_{max} stands for the biggest distribution function of beam-injected fast hydrogen ions. (a) From figure 6(a) with pitch value = 0.5; (b) from figure 6(b) with pitch value = 0.54.

Based on those assumptions and calculations, the MCI growth rate at any moment could be calculated. Figure 8 shows the MCI growth rate γ as a function of $\omega - k_{//} * v_d$ in the vicinity of cyclotron frequency Ω_b. The subscript b stands for fast beam-injected hydrogen ion in this manuscript. Both curves in figure 8 were obtained from Eq. (2), the red curve corresponding to 52 keV NBI-3 (1.8 MW) at 2.242 s, and the black curve corresponding to 71 keV NBI-8 (1.5 MW) at 2.206 s. Even though the NBI ions density with NBI-8 at t = 2.206 s ($\xi \approx 1.7 \times 10^{-3}$) is less than half of that with NBI-3 at t = 2.242 s ($\xi \approx 3.6 \times 10^{-3}$), the MCI growth rate for the 71 keV NBI-8 is higher. These simulation results agree well with the experimentally observed ICE energy in each NBI pulse shown in figure 4. This suggests that the core ICE excited by sub-Alfvénic beam-injected hydrogen ions in helium plasma is more sensitive to the beam-injected ion energy compared to the beam-injected ions density.

The propagation angle of the wave is assumed as θ = 84 °. It is based on the ICE growth rate which is about 10^4 as the ICE amplitude growth time $\triangle t$ is approximately $10^{-4}\ s$ shown in figure 9(a). The MCI growth rate γ is about 10^4 (almost the same with the ICE growth rate) at θ = 84 °, and it decreases very quickly as the propagation angle approaches θ = 90 ° shown in figure 9(b). It is necessary to point out that the γ drops back towards zero as the propagation angle approaches θ = 0 °, and the maximum value of γ is in the region of θ=70 ° to 80 °. This is no conflict with MCI theory as there is no compression Alfvénic wave and therefore no MCI at θ = 0 °.

Using the same theory of the MCI described previously, together with the fast ion distribution function obtained by TRANSP / NUBEAM shown in figure 11, the MCI growth rate γ around the end of NBI-3 (51 keV) could be calculated as shown in figure 10. In figure 11, the time of those four curves corresponding to the four asterisks with the same colour shown in figure 10(a). The red circles in figure 10(b) and the red squares in figure 10(c) stand for the maximum growth rates of MCI in the vicinity of Ω_b and 2 Ω_b. The time evolution of maximum MCI growth rates is shown in figure 10(d). It is obvious that the maximum MCI growth rates decrease very quickly after the NBI turn-off, which has the same changing trend as the ICE amplitudes shown in figure 5(b). In this specific case, the slowing down of the dominant beam ion velocity component and the spreading of the fast-ion distribution profile contribute to the stabilization of the MCI. The propagation angle of compression Alfvénic waves is also assumed as θ = 84°.

From figure 10(d), before the NBI turn-off (t = 2.242 s), the maximum MCI growth rate at the fundamental frequency is much larger than that at the second harmonic, which is also consistent with ICE amplitude shown in figure 5(b). However, the pre-appearing second harmonic ICE signal (before the red dashed line in figure 3(d)) cannot be explained by the linear MCI theory, as applied to the energetic ion distribution that we have considered. Further theoretical studies are needed to give an reasonable explanation for this unexpected phenomenon.

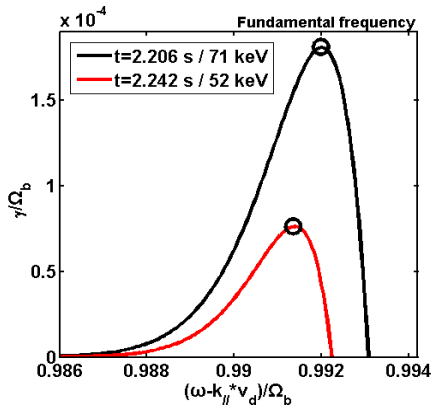

Figure 8. The MCI growth rate γ as a function of $\omega - k_{//} * v_d$ in the case of sub-Alfvénic hydrogen ions with the energy distribution shown in figure 6 and 7, the propagation angle of fast Alfvénic waves is assumed as θ = 84°. The red line corresponds to 52 keV NBI-3 at 2.242 s, the black line corresponds to 71 keV NBI-8 at 2.206 s.

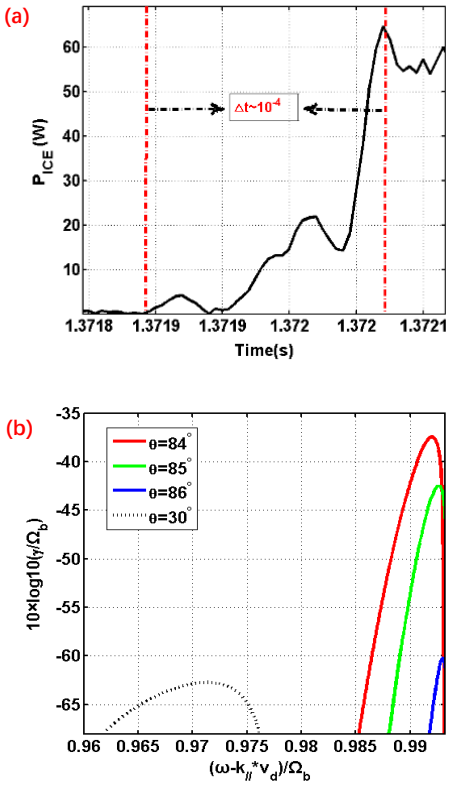

Figure 9. (a) The time evolution of ICE intensity, $\triangle t$ is the ICE amplitude growth time; (b) the value of MCI growth rates with the fast Alfvenic waves propagation angle θ = 84°, 85°, 86° and 30°. It is helium plasma heated by fast hydrogen ions with NBI-8 (71 keV) in shot 36719.

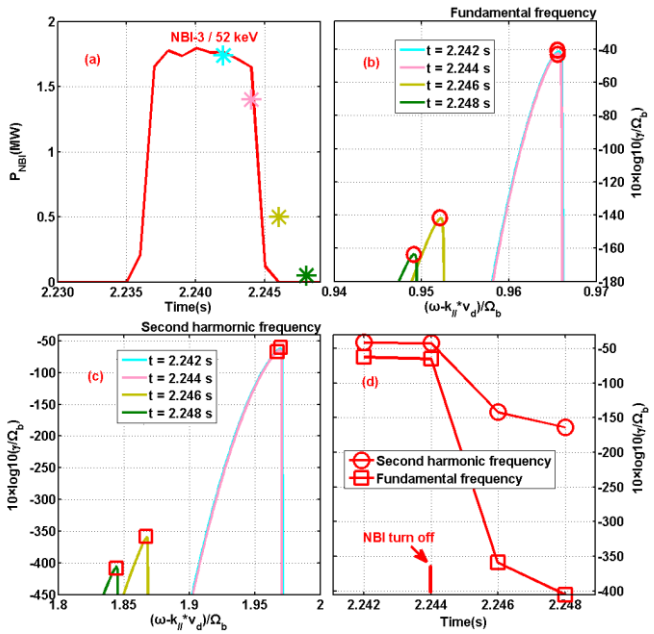

Figure 10. (a) The time evolution of NBI-8 power, asterisks correspond to the average power in 2 ms, which is used in TRANSP simulation; (b) and (c) show MCI growth rate γ in the vicinity of $\omega - k_{//} * v_d \approx \Omega_b$ and $\omega - k_{//} * v_d \approx 2\,\Omega_b$ respectively in the case of sub-Alfvénic beam-injected hydrogen ions in the plasma core, the red circles in (b) and the red squares in (c) shows the maximum growth rate values of MCI; (d) the time evolution of maximum MCI growth rates from (b) and (c). The propagation angle of fast Alfvénic waves is assumed as $\theta = 84°$.

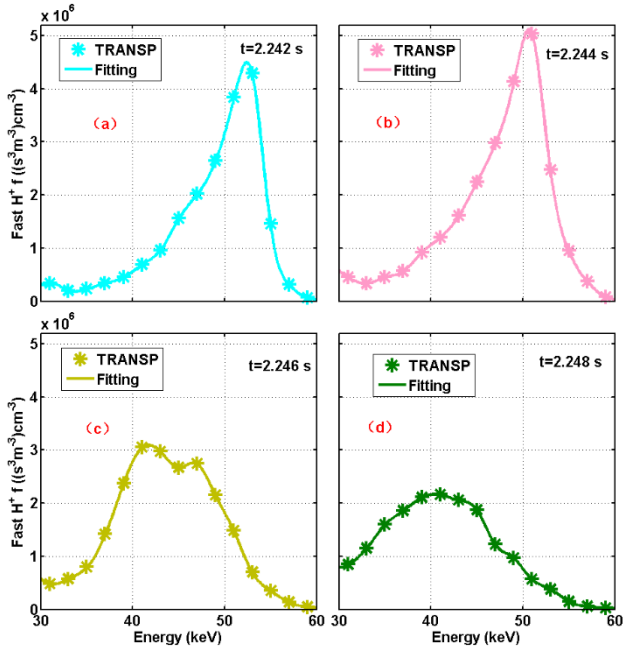

Figure 11. TRANSP-calculated beam ion energy distributions with pitch value = 0.54. Those four curves corresponding to the four asterisks with the same colour shown in figure 10 (a).

5. Summary

The excitation of core ICE, observed from helium plasma heated by sub-Alfvénic beam-injected hydrogen ions in ASDEX Upgrade is due to the MCI as the MCI growth rates are broadly consistent with the dynamics of ICE amplitudes: (1) the ICE amplitude is larger with 71 keV NBI-8 (1.5 MW) even though the power of it is lower compared to 52 keV NBI-3 (1.8 MW); (2) the ICE signals fall off rapidly after the NBI turn-off; (3) the ICE signal at the fundamental frequency is much larger than that at the second harmonic. The MCI growth rate is very sensitive to the energy and velocity distribution of beam-injected ions and is suppressed by the slowing down of the beam-injected ion velocity and the spreading of the fast ion distribution profile. The oblique propagation angle of MCI is taken as $\theta = 84^{\circ}$ based on the calculated MCI and the experimentally measured ICE growth rate. However, the pre-appearing second harmonic frequency of the ICE signal cannot be explained by the linear MCI theory. Further theoretical studies based on experimental results are needed to comprehensively describe this phenomenon. ICE is recommended as a potential diagnostic of fast ions in plasma for future fusion reactor devices, such as ITER, DEMO and CFETR, and this is supported by fully understanding the physical principle of ICE.

Acknowledgements

This work has been carried out within the framework of the EUROfusion Consortium and has received funding from the Euratom research and training programme 2014-2018, 2019-2020 under grant agreement No. 633053, the RCUK Energy Programme under grant No. EP/T012250/1 and National Natural Science Foundation of China under Grant No. 11975265, 11675213 and 11628509. The views and opinions expressed herein do not necessarily reflect those of the European Commission. The contribution of Rodolphe D'Inca to the development of the ICE diagnostic on ASDEX Upgrade is gratefully acknowledged.

References

[1] G.A. Cottrell, R.O. Dendy 1988 *Phys Rev Lett* **60** 33-36
[2] G.A. Cottrell, *et al.* 1993 *Nucl Fusion* **33** 1365-1387
[3] S. Cauffman, *et al.* 1995 *Nucl Fusion* **35** 1597
[4] R.O. Dendy, *et al.* 1995 *Nucl Fusion* **35** 1733-1742
[5] M. Ichimura, *et al.* 2008 *Nucl Fusion* **48** 035012
[6] R. Ochoukov, *et al.* 2018 *Rev Sci Instrum* **89** 10J101
[7] K.E. Thome, *et al.* 2018 *Rev Sci Instrum* **89** 10I102
[8] B. Chapman, *et al.* 2017 *Nucl Fusion* **57** 124004
[9] B. Chapman, *et al.* 2018 *Nucl Fusion* **58** 096027
[10] L.N. Liu, *et al.* 2019 *Rev Sci Instrum* **90** 063504
[11] B.C.G. Reman, *et al.* 2019 *Nucl Fusion* **59** 096013
[12] K.E. Thome, *et al.* 2019 *Nucl Fusion* **59** 086011
[13] R. Ochoukov, *et al.* 2019 *Nucl Fusion* **59** 014001

[14] B. Chapman, *et al.* 2020 *Plasma Phys Contr F* **62** 055003
[15] B. Chapman, *et al.* 2020 *Plasma Phys. Contr. F.* in press https://doi.org/10.1088/1361-6587/aba368
[16] L. Liu, *et al.* 2020 *Nucl Fusion* **60** 044002
[17] L.G. Askinazi, *et al.* 2018 *Nucl Fusion* **58** 082003
[18] H. Kimura, *et al.* 1998 *Nucl. Fusion* **38** 1303
[19] S. Sumida, *et al.* 2019 *Plasma Phys Contr F* **61** 025014
[20] M. Salewski, *et al.* 2016 *Nucl Fusion* **56** 106024
[21] M. Salewski, *et al.* 2014 *Nucl Fusion* **54** 023005
[22] M. Weiland, *et al.* 2016 *Plasma Phys Contr F* **58** 025012
[23] M. Weiland, *et al.* 2017 *Nucl Fusion* **57** 116058
[24] R.O. Dendy, C.N. Lashmore-Davies, K.F. Kam 1992 *Physics of Fluids B: Plasma Physics* **4** 3996-4006
[25] R.O. Dendy, C.N. Lashmore-Davies, K.G. McClements, G.A. Cottrell 1994 *Phys Plasmas* **1** 1918-1928
[26] K.G. McClements, *et al.* 1996 *Phys Plasmas* **3** 543-553
[27] J.W.S. Cook, R.O. Dendy, S.C. Chapman 2013 *Plasma Phys Contr F* **55** 065003
[28] L. Carbajal 2014 *Phys Plasmas* **21** 012106
[29] B. Chapman, *et al.* 2019 *Nucl Fusion* **59** 106021
[30] R. Ochoukov, *et al.* 2019 *Nucl Fusion* **59** 086032
[31] R.O. Dendy, K.G. McClements, C.N. Lashmore-Davies, R. Majeski, S. Cauffman 1994 *Phys Plasmas* **1** 3407-3413
[32] R.O. Dendy, C.N. Lashmoredavies, K.F. Kam 1992 *Phys Fluids B-Plasma* **4** 3996-4006
[33] K.G. McClements, *et al.* 2018 *Nucl Fusion* **58** 096020
[34] V.S. Belikov, I.I. Kolesnichenko, 1976 *Soviet Physics Technical Physics*
[35] N.N. Gorelenkov 2002 *Nucl Fusion* **42** 977
[36] https://www.ipp.mpg.de/16208/einfuehrung
[37] *An Introduction to Error Analysis: The Study of Uncertainties in Physical measurements, John R.Taylor, page:*122-126.
[38] D. Moseev, M. Salewski 2019 *Phys Plasmas* **26**
[39] H. Meyer et al. 2019 *Nucl. Fusion* **59** 112014
[40] B. Labit et al. 2019 *Nucl. Fusion* **59** 086020